Radio Science, Volume ???, Number , Pages 1–25,

Accurate 2.5-D Boundary Element Method for Conductive Media

Dieter Dobbelaere,[1] Hendrik Rogier[1] and Daniël De Zutter[1]

Corresponding author: D. Dobbelaere, Electromagnetics Group, Department of Information Technology, Ghent University, Sint-Pietersnieuwstraat 41, 9000 Ghent, Belgium. (dieter.dobbelaere@intec.ugent.be)

[1]Department of Information Technology,

Ghent University, Belgium.

The solution of the time-harmonic Maxwell equations using a boundary element method, for 2-D geometries illuminated by arbitrary 3-D excitations, gives rise to numerical difficulties if highly conductive media are present. In particular, the interaction integrals arising in the method of moments involve kernels that strongly oscillate in space and, at the same time, decay exponentially. We present an accurate method to tackle these issues over a very broad conductivity range (from lossy dielectric to conductor skin-effect regime), for both magnetic and non-magnetic conductors. Important applications are the modal analysis of waveguides with non-perfect conductors, scattering problems and shielding problems with enclosures with arbitrary permeability and conductivity and 3-D noise sources.

1. Introduction

Boundary element methods (BEMs) provide a powerful framework to solve the time-harmonic Maxwell equations numerically. If the problem domain consists of homogeneous material regions, a BEM generally requires fewer unknowns than a volumetric discretization technique. This paper considers two-dimensional geometries with conductive material regions, which can be magnetic, illuminated by arbitrary three-dimensional sources, leading to a so-called 2.5-D boundary element method. Important applications of this class of problems are propagation in uniform waveguides with non-perfect conductors [*Coluccini et al.*, 2013; *Tong et al.*, 2005; *Dobbelaere et al.*, 2013a], scattering problems [*Murphy et al.*, 1991] and shielding problems [*Dobbelaere et al.*, 2013b].

Interaction integrals appearing in the method of moments (MoM), with the scalar Green's function and its normal derivatives as kernels, are numerically challenging due to two specific and interplaying aspects. First, the kernels in good conductors are strongly oscillating and exponentially decaying in space, due to the large magnitude and imaginary part of the conductor's wave number w.r.t. the free space wave number. Second, the kernels are singular, or nearly singular, in those regions of the integration domain where the test and basis functions' supports overlap or lie close to each other, respectively. This behavior requires special care for an accurate numerical evaluation. Moreover, the combination of the two aspects, i.e. interaction integrals with both (nearly) singular and oscillating as well as exponentially damped integrands, poses

further difficulties. In this paper we present an accurate method to handle both problems.

A large amount of literature is available concerning the numerical evaluation of MoM interaction integrals in low-loss dielectric media. Integrals with singular or nearly singular integrands are usually evaluated with a singularity extraction [*Wilton et al.*, 1984; *Yla-Oijala and Taskinen*, 2003; *Graglia*, 1993] or cancellation technique [*Khayat and Wilton*, 2005; *Graglia and Lombardi*, 2008; *Polimeridis and Mosig*, 2010]. In 3-D, *Chakraborty and Jandhyala* [2004] use singularity cancellation with RWG basis functions [*Rao et al.*, 1982] to evaluate the interaction integrals in conductive media more accurately. A good overview of the additional problems that arise in conductive media can be found in *Peeters et al.* [2012], together with a singularity cancellation technique for the three-dimensional case.

To the authors' best knowledge, no accurate method for handling interaction integrals in conductive media for the 2.5-D case has been presented yet. This work proposes a new method specifically tailored to the properties of the 2.5-D Green's function in conductive media. It is shown, both theoretically and through corroborating examples, that the method accurately evaluates interaction integrals for a wide range of electrical conductivities (low-loss dielectric to highly conductive) and frequencies, and allows media with arbitrary permeability. In addition to the earlier mentioned fields of application, the new method is highly relevant to the accurate analysis of state-of-the-art multiconductor transmission lines and enclosures.

The structure of this paper is as follows: in Sections 2 and 3 we briefly outline the employed integral equations and the interaction integrals appearing in the MoM. The problems encountered in evaluating the integrals in conductive media are elaborated in Section 4, followed by our new method in Section 5. Finally, the numerical examples in Section 6 testify to the accuracy and applicability of the method, and clearly demonstrate the advantages over existing methods. Conclusions are formulated in Section 7.

2. Geometry and Boundary Integral Equations

Consider a 2-D geometry consisting of isotropic homogeneous material regions Ω_i, with permittivity $\epsilon_i \in \mathbb{C}$, permeability $\mu_i \in \mathbb{C}$ and boundary C_i (Fig. 1). Assume that all sources and fields have a common time and longitudinal dependence $e^{j(\omega t-\beta z)}$ ($\beta \in \mathbb{C}$), which is omitted for notational convenience. A general 3-D excitation can be expanded into sources of this kind via Fourier transformation in the z direction. The unknowns of the problem are the tangential electric and magnetic boundary fields, given by $\hat{\mathbf{n}} \times \mathbf{E} \times \hat{\mathbf{n}} = E_t \hat{\mathbf{t}} + E_z \hat{\mathbf{z}}$ and $\hat{\mathbf{n}} \times \mathbf{H} \times \hat{\mathbf{n}} = H_t \hat{\mathbf{t}} + H_z \hat{\mathbf{z}}$, with E_t and H_t the transverse tangential components, and E_z and H_z the longitudinal components. The following representation formulas hold [*Olyslager et al.*, 1993], with $E_t^{(i)} \hat{\mathbf{t}} + E_z^{(i)} \hat{\mathbf{z}}$ the incoming tangential electric field generated by sources in Ω_i, $\mathbf{r} = x\hat{\mathbf{x}} + y\hat{\mathbf{y}}$, and

$\gamma_i = \sqrt{\omega^2\epsilon_i\mu_i - \beta^2}$:

$$E_z(\mathbf{r}) = E_z^{(i)}(\mathbf{r}) + \oint_{C_i} \left[E_z(\mathbf{r}') \frac{\partial G_i(\mathbf{r}|\mathbf{r}')}{\partial n'} - \left(\frac{j\gamma_i^2}{\omega\epsilon_i} H_t(\mathbf{r}') - \frac{\beta}{\omega\epsilon_i} \frac{\partial H_z(\mathbf{r}')}{\partial t'} \right) G_i(\mathbf{r}|\mathbf{r}') \right] dc', \quad (1)$$

$$E_t(\mathbf{r}) = E_t^{(i)}(\mathbf{r}) + \oint_{C_i} \left[\frac{j\omega\mu_i}{\gamma_i^2} H_z(\mathbf{r}') \frac{\partial^2 G_i(\mathbf{r}|\mathbf{r}')}{\partial n \partial n'} - \frac{j\beta}{\gamma_i^2} E_z(\mathbf{r}') \frac{\partial^2 G_i(\mathbf{r}|\mathbf{r}')}{\partial t \partial n'} + \frac{j\omega\mu_i}{\gamma_i^2} \left(\frac{j\gamma_i^2}{\omega\mu_i} E_t(\mathbf{r}') - \frac{\beta}{\omega\mu_i} \frac{\partial E_z(\mathbf{r}')}{\partial t'} \right) \frac{\partial G_i(\mathbf{r}|\mathbf{r}')}{\partial n} + \frac{j\beta}{\gamma_i^2} \left(\frac{j\gamma_i^2}{\omega\epsilon_i} H_t(\mathbf{r}') - \frac{\beta}{\omega\epsilon_i} \frac{\partial H_z(\mathbf{r}')}{\partial t'} \right) \frac{\partial G_i(\mathbf{r}|\mathbf{r}')}{\partial t} \right] dc'. \quad (2)$$

Similar expressions for the magnetic field components are found with the duality substitutions $E \to H$, $H \to -E$, $\epsilon_i \to \mu_i$ and $\mu_i \to \epsilon_i$ in (1) and (2). With the choice $G_i(\mathbf{r}|\mathbf{r}') = \frac{j}{4} H_0^{(2)}(\gamma_i|\mathbf{r} - \mathbf{r}'|)$, the Green's function satisfies the Sommerfeld radiation condition at infinity, provided the branch cuts of γ_i are chosen such that $\Im\gamma_i \leq 0$.

A system of coupled integral equations is obtained after imposing continuity of the tangential fields at the boundaries, yielding a 2.5-D version of the PMCHWT (Poggio-Miller-Chang-Harrington-Wu-Tsai) operator [*Poggio and Miller*, 1973; *Chang and Harrington*, 1977; *Wu and Tsai*, 1977]. A finite-dimensional linear system is obtained with the MoM.

3. MoM Interaction Integrals

Before presenting our new theory from Section 4 onwards, we briefly recall which type of interaction integrals occur in the MoM of the 2.5-D PMCHWT boundary integral equation [*Olyslager et al.*, 1993; *Fostier et al.*, 2011]. The boundaries C_i are meshed into a union of segments S_j with length l_j, separated by nodes $\mathbf{r}_k$ (Fig. 2).

The transverse tangential components E_t and H_t are expanded in terms of pulse functions $p_j(\mathbf{r})$, with support over segment S_j, whereas the longitudinal components E_z and H_z are expanded into triangular functions $t_k(\mathbf{r})$, with support over segments that share a node $\mathbf{r}_k$ [*Olyslager et al.*, 1993; *Fostier et al.*, 2011]:

$$\begin{array}{ll} p_j(\mathbf{r}) = 1 & \mathbf{r} \in S_j, \\ t_k(\mathbf{r}) = 1 - |\mathbf{r} - \mathbf{r}_k| \; l_j^{-1} & \mathbf{r}, \mathbf{r}_k \in S_j. \end{array} \tag{3}$$

The continuity equations for E_z and H_z are tested with pulse functions, whereas the equations for E_t and H_t are tested with triangular functions. To calculate the elements in the MoM system matrix, the interaction integrals (4)-(6) below need to be evaluated numerically for basis and test functions with support over segments that have Ω_i as a neighboring medium. This can easily be seen by inspecting (1) and (2). The tangential derivatives of the Green's function can be transferred to the test function using integration by parts such that only three types of interaction integrals remain:

$$\mathsf{I}_{jk}^{(1)} = \int_{C_i} p_j(\mathbf{r}) dc \int_{C_i} G_i(\mathbf{r}|\mathbf{r}') \; p_k(\mathbf{r}') dc', \tag{4}$$

$$\mathsf{I}_{jk}^{(2)} = \int_{C_i} p_j(\mathbf{r}) dc \int_{C_i} \frac{\partial G_i(\mathbf{r}|\mathbf{r}')}{\partial n'} t_k(\mathbf{r}') dc', \tag{5}$$

$$\mathsf{I}_{jk}^{(3)} = \int_{C_i} t_j(\mathbf{r}) dc \int_{C_i} \frac{\partial^2 G_i(\mathbf{r}|\mathbf{r}')}{\partial n \partial n'} t_k(\mathbf{r}') dc'. \tag{6}$$

4. Difficulties in Conductive Media

Consider a conductive region Ω, with conductivity σ, complex permittivity $\epsilon = \epsilon_0 - j\frac{\sigma}{\omega}$ and permeability μ. The transversal wave number γ can be written as a function of the skin depth $\delta = \sqrt{2/(\omega\mu\sigma)}$ for moderate to high conductivity values,

as follows:

$$\gamma = \sqrt{\omega^2\mu(\epsilon_0 - j\sigma/\omega) - \beta^2} \tag{7}$$

$$\underset{\sigma \gg \omega\epsilon_0}{\approx} \frac{1-j}{\delta}. \tag{8}$$

The particular form of this wave number is responsible for the difficulties that arise in evaluating the interaction integrals (4)-(6) in a highly conductive medium. The Green's function in the conductor reduces to $\frac{j}{4}H_0^{(2)}\left((1-j)r/\delta\right)$, with $r = |\mathbf{r} - \mathbf{r}'|$, while its normal derivatives are expressible in terms of the zeroth, first and second order Hankel functions of the second kind (see appendix A). For large $|\gamma r|$, the Hankel function of the second kind and order ν behaves as [*Watson*, 1995]

$$H_\nu^{(2)}(\gamma r) \sim \left(\frac{2}{\pi\gamma r}\right)^{\frac{1}{2}} e^{-j\gamma r + j\frac{\pi}{4}(2\nu+1)} \qquad (|\arg \gamma r| < \pi). \tag{9}$$

In a highly conductive medium, the large imaginary part of the wave number causes a strong exponential decay of the Green's function and its derivatives. Moreover, the wavelength $\lambda = 2\pi\delta$ is small w.r.t. the free space wavelength, which leads to a spatially strong oscillation of the Green's function and its derivatives. If S_j is a segment on the interface between the conductive region Ω and a dielectric region Ω_d, it is sufficient to choose the segment length to be a fraction of the wavelength λ_d in the dielectric, say $l_j = \frac{\lambda_d}{10} = \frac{2\pi}{10\omega\sqrt{\epsilon_d\mu_d}}$, in order to capture the varying field behavior at the interface. This is because the tangential fields at the interface can only vary at a pace on the order of λ_d in the dielectric and remain continuous at the interface (there are no surface currents). Typically $\delta \ll l_j$ and accordingly a lot of oscillations occur along one segment and standard quadrature techniques fail

to correctly evaluate the interaction integrals in the conductive region. Choosing $l_j = \frac{\lambda}{10}$ (with λ corresponding to the wavelength in the conductor) to try to tackle this problem is unnecessary to capture the field behavior and would lead to a very large increase of the number of unknowns.

5. Accurate Evaluation of MoM Interaction Integrals

This section proposes a new method to accurately evaluate the MoM interaction integrals in conductive media, with a relatively low quadrature order. The method reduces to the traditional approach in *Fostier et al.* [2011] for $\sigma \ll \omega\epsilon_0$ (low-loss dielectric case), and is therefore applicable to arbitrary conductivities $\sigma \in [0, \infty[$, as shown in this section and corroborated by the numerical examples in Section 6.

5.1. Cutoff Distance

The key to accurately integrate the strongly oscillating and exponentially decaying integrands in conductive media, for a fixed number of quadrature points, is to distribute those points over the integration domain where the Green's function has a non-negligible value. Because the magnitude of the Green's function decays exponentially in a good conductor, it can be approximated as $\frac{j}{4}H_0^{(2)}(\gamma r)\mathbb{H}(r_{\mathsf{cut}} - r)$, neglecting its tail, with $\mathbb{H}$ the Heaviside step function and r_{cut} the cutoff distance.

The cutoff distance is the distance above which the asymptotic Green's function (using (9)) becomes smaller in magnitude than a threshold Δ_{cut}. It can be written in terms of the principal branch of the Lambert W function, denoted $\mathcal{W}(z)$.

Definition 1 (Cutoff distance r_{cut})**.**

$$r_{\mathsf{cut}} = -\frac{1}{2\Im\gamma}\mathcal{W}\left(\frac{-4\Im\gamma}{\pi\Delta_{\mathsf{cut}}^2|\gamma|}\right) \underset{\sigma\gg\omega\epsilon_0}{\approx} \frac{\delta}{2}\mathcal{W}\left(\frac{2\sqrt{2}}{\pi\Delta_{\mathsf{cut}}^2}\right) \tag{10}$$

An upper bound on the Green's function itself is given in Theorem 5.1. For sufficiently small Δ_{cut}, the asymptotic expansion (9) is a good approximation and $C \approx 1$.

Theorem 5.1. *For $r \geq r_{\mathsf{cut}}$ the following inequality holds: $|G(r)| \leq C\Delta_{\mathsf{cut}}e^{(r-r_{\mathsf{cut}})\Im\gamma}$ with $C = 1 + \frac{1}{8|\gamma|r_{\mathsf{cut}}}$.*

Proof. Note that $H_0^{(2)}(z) = \sqrt{\frac{2}{\pi z}}e^{-j\left(z-\frac{\pi}{4}\right)}\left(1 - \frac{\theta_2(z)}{8jz}\right)$, with $|\theta_2(z)| < 1$ if $\Im z < 0$ [*Gradshteyn and Ryzhik*, 2007]. For $r \geq r_{\mathsf{cut}}$, this leads to

$$\left|\frac{j}{4}H_0^{(2)}(\gamma r)\right| \leq \frac{1}{4}\sqrt{\frac{2}{\pi|\gamma|r_{\mathsf{cut}}}}e^{r_{\mathsf{cut}}\Im\gamma}e^{(r-r_{\mathsf{cut}})\Im\gamma}\left(1 + \frac{1}{8|\gamma|r_{\mathsf{cut}}}\right) \tag{11}$$

$$= C\Delta_{\mathsf{cut}}e^{(r-r_{\mathsf{cut}})\Im\gamma}, \tag{12}$$

where the last step follows from Definition 1. □

To illustrate the use of the cutoff distance in the calculation of the interaction integrals, consider $\mathsf{I}_{jk}^{(1)}$ in a conductive medium:

$$\mathsf{I}_{jk}^{(1)} \approx \int_{S_j} p_j(\mathbf{r})dc \int_{S_k} G(\mathbf{r}|\mathbf{r}')\mathbb{H}(r_{\mathsf{cut}} - |\mathbf{r} - \mathbf{r}'|)p_k(\mathbf{r}')dc'. \tag{13}$$

The boundaries of the test integral over test segment S_j follow from the intersection of S_j with the set of points that are closer than the cutoff distance from the source segment S_k (region Υ_k in Fig. 3). Because Υ_k is convex, either $S_j \cap \Upsilon_k = \varnothing$ (no interaction) or $S_j \cap \Upsilon_k$ is a subsegment (AB in Fig. 3). For each test point $\mathbf{r} \in (S_j \cap \Upsilon_k)$, the basis integration interval is a subsegment of S_k (CD in Fig. 4).

In this way, interactions between points that are separated further than r_{cut} are neglected and the quadrature points are distributed over the region where the in-

tegrand is non-negligible, which alleviates the problem of the exponential damping of the integrand. At the same time, the number of oscillations of the integrands in the interaction integrals is small, *independent of the conductivity*, allowing a relatively low quadrature order. To show this, consider an interface between free space (wavelength λ_0) and a conductive region (conductivity σ, wave number $\gamma = \sqrt{\omega^2\mu_0(\epsilon_0 - j\sigma/\omega) - \beta^2}$), with boundary segment length equal to $l = \lambda_0/10$. The integrands of the interaction integrals (4)-(6) can be expressed in terms of Hankel functions of the second kind, as shown in (15). For $\sigma \gg \omega\epsilon_0$, it is evident from (10) that $r_{\mathsf{cut}} \sim \delta$, implying that the number of oscillations of $H_\eta^{(2)}(\gamma r)$ in $r \in [0, r_{\mathsf{cut}}]$ is bounded for high conductivities. For $\sigma \ll \omega\epsilon_0$, $r_{\mathsf{cut}} > l$ and the number of oscillations of $H_\eta^{(2)}(\gamma r)$ for $r \in [0, l]$ in a dielectric region is also bounded. A measure for the maximum number of oscillations of the integrands is given by

$$Z = \max_{\substack{\sigma\in[0,\infty[\\ \beta\in[0,\omega\sqrt{\epsilon_0\mu_0}] \\ \eta\in\{0,1,2\} \\ \mathcal{P}\in\{\Re,\Im\}}} z(\mathcal{P}H_\eta^{(2)}(\gamma r), [0, \min(r_{\mathsf{cut}}, l)]), \tag{14}$$

where $z(f(r), \mathcal{A})$ denotes the number of zero-crossings of $f(r)$ in $r \in \mathcal{A}$. It can be easily verified that $Z = 2$, 4 and 6 if $\Delta_{\mathsf{cut}} = 10^{-3}$, 10^{-6} and 10^{-9}, respectively, which shows that the number of oscillations increases if a higher accuracy is required (larger r_{cut}), but remains small, allowing a low quadrature order, independent of σ. In conclusion, the cutoff distance alleviates both problems of exponentially damped and highly oscillatory kernels in conductive media. This approach is an extension of the traditional method in *Fostier et al.* [2011], to accurately evaluate the interaction integrals in media with arbitrary conductivity.

5.2. Singularity Extraction

The three types of interaction integrals (4)-(6) can be written as

$$\mathsf{I}_{jk}^{(l)} = \int_{C_i} w_j^{(l)}(\mathbf{r}) \int_{C_i} b_k^{(l)}(\mathbf{r}')\mathbb{H}(r_{\mathsf{cut}} - r) \sum_{\eta=0}^{2} f_\eta^{(l)}(\mathbf{r},\mathbf{r}')H_\eta^{(2)}(\gamma r)dc'\ dc. \tag{15}$$

The test and basis functions are given by

$$w_j^{(1)}(\mathbf{r}) = w_j^{(2)}(\mathbf{r}) = p_j(\mathbf{r}), \tag{16}$$

$$w_j^{(3)}(\mathbf{r}) = t_j(\mathbf{r}), \tag{17}$$

$$b_k^{(1)}(\mathbf{r}') = p_k(\mathbf{r}'), \tag{18}$$

$$b_k^{(2)}(\mathbf{r}') = b_k^{(3)}(\mathbf{r}') = t_k(\mathbf{r}'). \tag{19}$$

As shown in appendix A, the functions $f_\eta^{(l)}(\mathbf{r},\mathbf{r}')$ that are not identically zero are given by

$$f_0^{(1)} = \frac{j}{4}, \tag{20}$$

$$f_1^{(2)} = \frac{j\gamma}{4}(\hat{\mathbf{n}}' \cdot \hat{\mathbf{r}}), \tag{21}$$

$$f_0^{(3)} = \frac{j\gamma^2}{8}(\hat{\mathbf{n}} \cdot \hat{\mathbf{n}}'), \tag{22}$$

$$f_2^{(3)} = \frac{j\gamma^2}{8}\left(\hat{\mathbf{n}} \cdot \hat{\mathbf{n}}' - 2(\hat{\mathbf{n}} \cdot \hat{\mathbf{r}})(\hat{\mathbf{n}}' \cdot \hat{\mathbf{r}})\right). \tag{23}$$

If the test and basis functions' supports overlap or lie next to each other, the integrands in (15) have a singularity in the integration domain. We employ a singularity extraction technique with an extracted singular part that is also limited by the cutoff distance, given by

$$\mathsf{I}_{jk,\mathsf{sing}}^{(l)} = \int_{C_i} w_j^{(l)}(\mathbf{r}) \int_{C_i} b_k^{(l)}(\mathbf{r}')\mathbb{H}(r_{\mathsf{cut}} - r) \sum_{\eta=0}^{2} f_\eta^{(l)}(\mathbf{r},\mathbf{r}')\mathcal{S}_\eta(\gamma r)dc'\ dc. \tag{24}$$

The functions $\mathcal{S}_\eta$ are given by

$$\mathcal{S}_0(\gamma r) = -\frac{2j}{\pi}\log r, \tag{25}$$

$$\mathcal{S}_1(\gamma r) = \frac{2j}{\pi\gamma r}, \tag{26}$$

$$\mathcal{S}_2(\gamma r) = \frac{4j}{\pi\gamma^2 r^2}. \tag{27}$$

The integrals of the limited singular parts are known in closed-form. For example, the self-patch term of the first type is given by

$$\mathsf{I}^{(1)}_{jj,\mathsf{sing}} = -\frac{j}{\pi}a((4l_j - 2a)\log a - 4l_j + a), \tag{28}$$

with $a = \min(r_{\mathsf{cut}}, l_j)$.

6. Numerical Results

Plane wave scattering at a conductive cylinder is used to validate the accuracy of the proposed method as a function of the accuracy parameter Δ_{cut}, for a wide range of electrical conductivities in the general case of oblique incidence ($\beta \neq 0$), and to compare it with existing methods. The next examples are practically relevant shielding problems, in which a conductive and (non-)magnetic enclosure with apertures is used to shield the interior from the fields generated by an exterior electric current source. The new method is able to accurately calculate the shielding performance over a broad frequency range, and outperforms existing methods in terms of accuracy and simulation time.

6.1. Scattering at a Conductive Cylinder

To validate the accuracy of the proposed 2.5-D BEM for conductive media and compare it with existing numerical methods, we consider the problem of plane wave scattering at a conductive cylinder (diameter d, finite conductivity σ and permittivity $\epsilon_0 - j\sigma/\omega$), embedded in free space (Fig. 5). An analytical expression of the solution can be obtained via separation of variables [*Van Bladel*, 2007]. The accuracy of the proposed method is compared with the traditional method without cutoff distance, and with a surface impedance approximation, over a wide conductivity range, from the low-loss dielectric ($\omega\epsilon_0 \gg \sigma$) to the conductive region ($\omega\epsilon_0 \ll \sigma$).

The numerically obtained radar cross section (RCS), denoted $S_n(\phi)$, is compared with the analytical solution, denoted $S_a(\phi)$. The relative error between these cross sections is defined by

$$\mathcal{E} = \sqrt{\frac{\sum_{k=1}^{K} |S_n(\phi_k) - S_a(\phi_k)|^2}{\sum_{k=1}^{K} |S_a(\phi_k)|^2}}, \tag{29}$$

with $\phi_k = 2\pi k/K$ and $K = 100$. Figures 6-7 show the relative error as a function of the skin depth for the two polarizations (VV and VH) of oblique plane wave incidence ($\alpha = 45°$). The skin depth $\delta = \sqrt{2/(\omega\mu_0\sigma)}$ ranges from 10^{-5} m to 10 m, covering the region between a good conductor with conductivity $\sigma = 10^7$ S/m and a low-loss dielectric with relative dielectric constant $1 - 5 \cdot 10^{-4} j$. Observe that, in general, the error decreases if the accuracy threshold Δ_{cut} becomes smaller. The relative error saturates around five significant digits for small and large skin depths, but this lower bound is determined mostly by the boundary meshing of the circular cross section into straight segments. The asymptotic value for the cutoff distance in (10), in case of

high conductivity, is shown in the legend. For $r_{\mathsf{cut}} > d$, no interactions are neglected, and the numerical solution becomes independent of Δ_{cut}, as can be seen for high δ/d values.

The inability of the traditional method without cutoff distance (i.e. the proposed method with $r_{\mathsf{cut}} = \infty$) to accurately evaluate the interaction integrals in conductive media, for a fixed quadrature order and constant number of boundary segments, is clearly demonstrated in Fig. 7. The problems mentioned in Section 4, i.e. the exponential decay combined with strong oscillation of the integrands, render the traditional method inaccurate or useless for low values of δ/d. The proposed method focuses the quadrature points in the region where the integrands are non-negligible, by introducing the cutoff distance (10) and a singularity extraction with limited extracted part, which in turn limits the number of oscillations. This leads to a near constant accuracy over the considered conductivity range (if enough oscillations are taken into account, i.e. for sufficiently low Δ_{cut}). For $r_{\mathsf{cut}} > d$, or equivalently for high δ/d values, our new method reduces to the traditional one, and the numerical solution is the same for both methods.

Another approach to incorporate good conductors in a BEM is the use of a surface impedance approximation, by imposing the condition $\mathbf{E} \times \hat{\mathbf{n}} = Z_s(\hat{\mathbf{n}} \times \mathbf{H} \times \hat{\mathbf{n}})$ on the conductor boundary, with $Z_s = (1+j)\sqrt{\frac{\omega\mu_0}{2\sigma}}$ and $\hat{\mathbf{n}}$ the outward normal to the conductive region. Figures 6-7 show that this is a good approximation for low values of δ/d, i.e. in the conductor skin-effect regime (note that the error does not saturate around 100 dB because the analytical solution with surface impedance approximation

is considered). It is apparent from Fig. 7 that the proposed method (with $\Delta_{\mathsf{cut}} = 10^{-9}$) outperforms the surface impedance approximation and traditional method in terms of accuracy, in the transition region between low-loss dielectric and skin-effect regime.

6.2. Slotted Coaxial Shield

In this example, we investigate the shielding performance of a coaxial enclosure with one or two slots at angles α_1 and α_2 (Fig. 8). The coaxial enclosure is illuminated by an electric line current $I_0\delta(\mathbf{r} - \mathbf{r}_0)\hat{\mathbf{z}}$ (hence $\beta = 0$), which induces an unwanted noise current I_1 in the enclosed copper signal conductor. Remark that, in addition to our MoM integral equation technique, scattering at a concentrically loaded cylindrical shield with $n - 1$ apertures can be solved by reducing an n-series problem to an equivalent Riemann-Hilbert problem [*Ziolkowski*, 1985; *Ziolkowski and Grant*, 1987]. A similar radial mode matching technique has been employed for multi-slotted shields with finite thickness [*Lee et al.*, 2012]. We consider three enclosure materials: copper ($\sigma = 5.8 \cdot 10^7$ S/m, $\mu_r = 1$), a magnetic conductor with the same skin depth ($\sigma = 5.8 \cdot 10^4$ S/m, $\mu_r = 1000$), and a perfect electric conductor ($\sigma = \infty$). The configurations with one and two slots are described by $\alpha_1 = 90^\circ$ and $(\alpha_1, \alpha_2) = (60^\circ, 120^\circ)$, respectively.

Figure 9 shows the relative noise current amplitude $|I_1/I_0|$ of the copper and perfect electric conducting (PEC) enclosure, over a broad frequency range (from 100 Hz to 1 GHz). Observe that the analytical solution for the closed coaxial enclosure (no slots) coincides with the numerical solution. At low frequencies, there is leakage

through the copper enclosure, as the skin depth is comparable to the thickness, and the presence of slots does not deteriorate the shielding performance significantly. At high frequencies, the predominant leakage mechanism is diffraction of the fields at the slots, and the copper and PEC shields exhibit the same behavior. For the given position of the slots and line current, the noise current for two slots is about 15 dB higher than for one slot.

Figure 10 shows the relative noise current amplitude for the magnetic conducting enclosure. For the configuration without slots, the numerical and analytical solution coincide. Compared to the copper enclosure, at low frequencies, the presence of slots now has a larger influence. This is due to a different shielding mechanism in the magnetic conductor, adding to the effect of the conductivity. If $\mu_r > 1$, the magnetic induction produced by the source is diverted into the enclosure, then shunted within the material in a direction nearly parallel to its surface, and finally released back into free space [*Celozzi et al.*, 2008]. The presence of slots disturbs the flux shunting, and negatively affects the shielding performance.

It is interesting to compare our new method with the traditional method ($r_{\mathsf{cut}} = \infty$) in terms of accuracy and simulation time. Fig. 11 shows the calculated shielding performance as a function of the quadrature order Q, for the copper shield with two slots. For $\Delta_{\mathsf{cut}} = 10^{-9}$, the new method already converges to the solution for $Q = 10$, compared to $Q = 80$ for the traditional method. For the same quadrature order $Q = 10$, the traditional method fails to accurately predict the shielding performance, due to the problems mentioned in Section 4. Evidently, the need for a smaller quadrature

order to obtain the same accuracy leads to a decrease in simulation time (Table 1). Even for the same quadrature order ($Q = 10$), our method is faster than the traditional method because interactions between segments separated by at least the cutoff distance are not taken into account.

6.3. Cable Tray Shield

The geometry of a metal cable tray with polygonal cross section (Fig. 12) is similar to the previous example, but arguably more interesting from a practical perspective. In this case, no closed-form analytical solution is available for the closed cable tray ($g = 0$). The enclosure is illuminated by an electric line current $I_0\delta(\mathbf{r} - \mathbf{r}_0)\hat{\mathbf{z}}$ (hence $\beta = 0$), which induces unwanted noise currents I_i in the three copper signal conductors. Figure 13 shows the relative current magnitude $|I_2/I_0|$ in the middle conductor, for an open and closed cable tray (aperture length $g = 5.5$ mm and $g = 0$, respectively). We consider three enclosure materials: copper ($\sigma = 5.8 \cdot 10^7$ S/m, $\mu_r = 1$), a magnetic conductor with the same skin depth ($\sigma = 5.8 \cdot 10^4$ S/m, $\mu_r = 1000$), and a perfect electric conductor ($\sigma = \infty$).

At low frequencies (up to 10^5 Hz), we notice that the influence of the apertures can be neglected, as the open and closed cable tray yield approximately the same shielding performance, for both copper and the magnetic conductor. In this region, the skin depth is comparable to the thickness, allowing the fields to penetrate the enclosure. At high frequencies, the copper and perfectly conducting open cable tray behave in the same way, indicating that diffraction of the fields through the aperture

is the predominant leakage mechanism. Observe that the magnetic conductor exhibits a worse shielding performance than copper, for all considered frequencies.

7. Conclusions

This paper presents a novel method to accurately and efficiently calculate 2.5-D MoM interactions integrals in conductive media, with arbitrary permeability. The resulting BEM is practically relevant to a large number of application domains, including modal analysis of waveguides with non-perfect conductors, scattering problems, and shielding problems with general three-dimensional sources.

Appendix A: Derivation of the Green's function's normal derivatives

Using the notation of Figure 14, the gradients of the Green's function $G(\mathbf{r}|\mathbf{r}') = \frac{j}{4}H_0^{(2)}(\gamma r)$ w.r.t. the observation point $\mathbf{r}$ and source point $\mathbf{r}'$ are given by

$$\boldsymbol{\nabla} G(\mathbf{r}|\mathbf{r}') = -\boldsymbol{\nabla}' G(\mathbf{r}|\mathbf{r}') = -\frac{j\gamma}{4} H_1^{(2)}(\gamma r)\hat{\mathbf{r}}. \tag{A1}$$

From these expressions, the normal derivatives of the Green's function follow immediately:

$$\frac{\partial G}{\partial n}(\mathbf{r}|\mathbf{r}') = -\frac{j\gamma}{4} H_1^{(2)}(\gamma r)(\hat{\mathbf{n}} \cdot \hat{\mathbf{r}}), \tag{A2}$$

$$\frac{\partial G}{\partial n'}(\mathbf{r}|\mathbf{r}') = \frac{j\gamma}{4} H_1^{(2)}(\gamma r)(\hat{\mathbf{n}'} \cdot \hat{\mathbf{r}}). \tag{A3}$$

Taking the gradient w.r.t. $\mathbf{r}'$ of (A1) leads to the following dyadic, with the dot representing the derivative of a holomorphic function:

$$\begin{aligned} \boldsymbol{\nabla}'\boldsymbol{\nabla} G(\mathbf{r}|\mathbf{r}') &= \boldsymbol{\nabla}' \left(\frac{j\gamma}{4} \dot{H}_0^{(2)}(\gamma r) \right) \hat{\mathbf{r}} + \frac{j\gamma}{4} \dot{H}_0^{(2)}(\gamma r) \boldsymbol{\nabla}' \hat{\mathbf{r}} \\ &= -\frac{j\gamma^2}{4} \ddot{H}_0^{(2)}(\gamma r) \hat{\mathbf{r}}\hat{\mathbf{r}} - \frac{j\gamma}{4r} \dot{H}_0^{(2)}(\gamma r) \hat{\boldsymbol{\phi}}\hat{\boldsymbol{\phi}}. \end{aligned} \tag{A4}$$

After some manipulations, the second order normal derivative of the Green's function can finally be written as

$$\begin{aligned} \frac{\partial^2 G}{\partial n \partial n'}(\mathbf{r}|\mathbf{r}') &= \hat{\mathbf{n}'} \cdot \boldsymbol{\nabla}'\boldsymbol{\nabla} G \cdot \hat{\mathbf{n}} \\ &= \frac{j\gamma^2}{8} \left(H_0^{(2)}(\gamma r) + H_2^{(2)}(\gamma r) \right) \hat{\mathbf{n}} \cdot \hat{\mathbf{n}'} - \frac{j\gamma^2}{4} H_2^{(2)}(\gamma r)(\hat{\mathbf{n}} \cdot \hat{\mathbf{r}})(\hat{\mathbf{n}'} \cdot \hat{\mathbf{r}}). \end{aligned} \tag{A5}$$

Acknowledgments. This work is partially supported by the Research Foundation Flanders (FWO-V) and by BELSPO through the IAP Phase VII BESTCOM project. The data of the numerical examples can be obtained by contacting the corresponding

303 author. The authors are grateful to the editor and the anonymous reviewers for their
304 valuable comments.

References

305 Celozzi, S., R. Araneo, and G. Lovat (2008), *Electromagnetic Shielding*, Wiley Series
306 in Microwave and Optical Engineering, John Wiley & Sons.

307 Chakraborty, S., and V. Jandhyala (2004), Evaluation of Green's function integrals
308 in conducting media, *Antennas and Propagation, IEEE Transactions on*, *52*(12),
309 3357 – 3363, doi:10.1109/TAP.2004.836430.

310 Chang, Y., and R. Harrington (1977), A surface formulation for characteristic modes
311 of material bodies, *Antennas and Propagation, IEEE Transactions on*, *25*(6), 789
312 – 795, doi:10.1109/TAP.1977.1141685.

313 Coluccini, G., M. Lucido, and G. Panariello (2013), Spectral domain analysis of
314 open single and coupled microstrip lines with polygonal cross-section in bound and
315 leaky regimes, *Microwave Theory and Techniques, IEEE Transactions on*, *61*(2),
316 736–745, doi:10.1109/TMTT.2012.2231424.

317 Dobbelaere, D., H. Rogier, and D. De Zutter (2013a), Properties and nu-
318 merical solutions of dispersion curves in general isotropic waveguides, *Mi-*
319 *crowave Theory and Techniques, IEEE Transactions on*, *61*(9), 3161–3168, doi:
320 10.1109/TMTT.2013.2273760.

321 Dobbelaere, D., H. Rogier, and D. De Zutter (2013b), Accurate 2D MoM technique
322 for arbitrary dielectric, magnetic and conducting media applied to shielding prob-

lems, in *Electromagnetic Theory (EMTS), Proceedings of 2013 URSI International Symposium on*, pp. 738–741.

Fostier, J., B. Michiels, I. Bogaert, and D. D. Zutter (2011), A Fast 2D Parallel MLFMA Solver for Oblique Plane Wave Incidence, *Radio Science*.

Gradshteyn, I. S., and I. M. Ryzhik (2007), *Table of Integrals, Series and Products, seventh edition*, Academic Press.

Graglia, R. (1993), On the numerical integration of the linear shape functions times the 3-D Green's function or its gradient on a plane triangle, *Antennas and Propagation, IEEE Transactions on*, *41*(10), 1448 –1455, doi:10.1109/8.247786.

Graglia, R., and G. Lombardi (2008), Machine precision evaluation of singular and nearly singular potential integrals by use of Gauss quadrature formulas for rational functions, *Antennas and Propagation, IEEE Transactions on*, *56*(4), 981 –998, doi:10.1109/TAP.2008.919181.

Khayat, M., and D. Wilton (2005), Numerical evaluation of singular and near-singular potential integrals, *Antennas and Propagation, IEEE Transactions on*, *53*(10), 3180 – 3190, doi:10.1109/TAP.2005.856342.

Lee, W.-S., H.-L. Lee, H.-S. Jang, H.-S. Tae, and J.-W. Yu (2012), Analysis of scattering with multi-slotted cylinder with thickness: TM case, *Progress In Electromagnetics Research*, *128*, 105–120.

Murphy, R. A., C. G. Christodoulou, and R. L. Phillips (1991), Electromagnetic scattering from a finite cylinder with complex permittivity, *Proc. SPIE*, *1558*, 295–305, doi:10.1117/12.49635.

345 Olyslager, F., D. De Zutter, and K. Blomme (1993), Rigorous analysis of the propaga-
346 tion characteristics of general lossless and lossy multiconductor transmission lines
347 in multilayered media, *Microwave Theory and Techniques, IEEE Transactions on*,
348 *41*(1), 79 –88, doi:10.1109/22.210232.

349 Peeters, J., I. Bogaert, and D. De Zutter (2012), Calculation of MoM interaction in-
350 tegrals in highly conductive media, *Antennas and Propagation, IEEE Transactions*
351 *on*, *60*(2), 930–940, doi:10.1109/TAP.2011.2173105.

352 Poggio, A., and E. Miller (1973), Integral equation solution of three-dimensional scat-
353 tering problems, in *Computer Techniques for Electromagnetics*, edited by R. Mittra,
354 chap. 4, Pergamon Press.

355 Polimeridis, A., and J. Mosig (2010), Evaluation of weakly singular integrals
356 via generalized cartesian product rules based on the double exponential for-
357 mula, *Antennas and Propagation, IEEE Transactions on*, *58*(6), 1980 –1988, doi:
358 10.1109/TAP.2010.2046866.

359 Rao, S., D. Wilton, and A. Glisson (1982), Electromagnetic scattering by surfaces of
360 arbitrary shape, *Antennas and Propagation, IEEE Transactions on*, *30*(3), 409 –
361 418, doi:10.1109/TAP.1982.1142818.

362 Tong, M., G. Pan, and G. Lei (2005), Full-wave analysis of coupled lossy transmission
363 lines using multiwavelet-based method of moments, *Microwave Theory and Tech-*
364 *niques, IEEE Transactions on*, *53*(7), 2362–2370, doi:10.1109/TMTT.2005.850438.

365 Van Bladel, J. (2007), *Electromagnetic Fields*, The IEEE Press Series on Electromag-
366 netic Wave Theory, second ed., Wiley.

Watson, G. (1995), *A Treatise on the Theory of Bessel Functions*, Cambridge Mathematical Library, Cambridge University Press.

Wilton, D., S. Rao, A. Glisson, D. Schaubert, O. Al-Bundak, and C. Butler (1984), Potential integrals for uniform and linear source distributions on polygonal and polyhedral domains, *Antennas and Propagation, IEEE Transactions on*, *32*(3), 276 – 281, doi:10.1109/TAP.1984.1143304.

Wu, T., and L. Tsai (1977), Scattering from arbitrarily-shaped lossy dielectric bodies of revolution, *Radio Science*, pp. 709–718.

Yla-Oijala, P., and M. Taskinen (2003), Calculation of CFIE impedance matrix elements with RWG and n $\times$ RWG functions, *Antennas and Propagation, IEEE Transactions on*, *51*(8), 1837 – 1846, doi:10.1109/TAP.2003.814745.

Ziolkowski, R. (1985), n-Series problems and the coupling of electromagnetic waves to apertures: A Riemann-Hilbert approach, *SIAM Journal on Mathematical Analysis*, *16*(2), 358–378, doi:10.1137/0516026.

Ziolkowski, R., and J. Grant (1987), Scattering from cavity-backed apertures: The generalized dual series solution of the concentrically loaded E-pol slit cylinder problem, *Antennas and Propagation, IEEE Transactions on*, *35*(5), 504–528, doi:10.1109/TAP.1987.1144143.

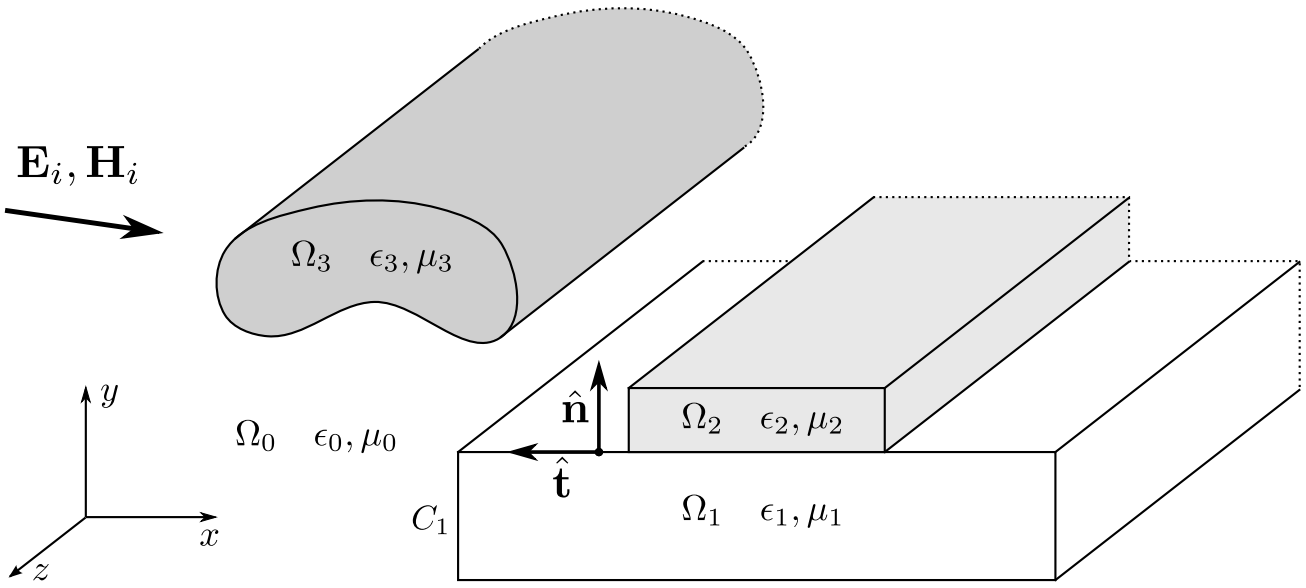

Figure 1. General isotropic piecewise-homogeneous 2-D geometry with a 3-D excitation.

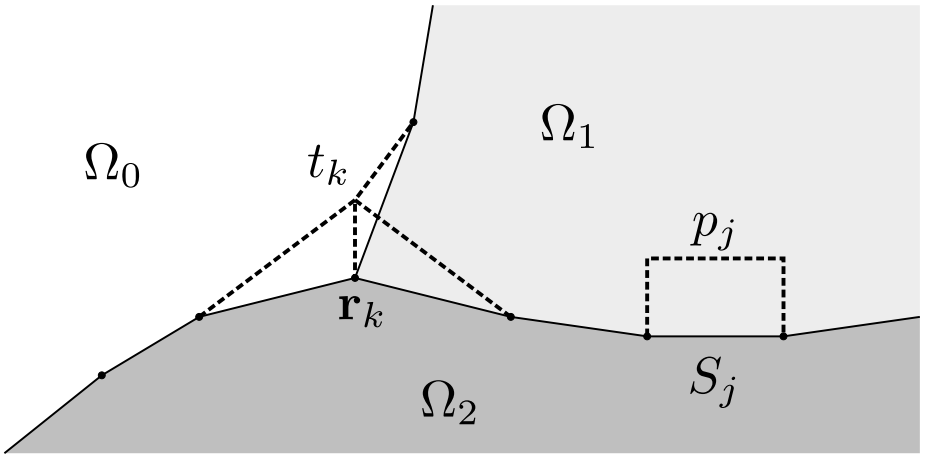

Figure 2. The boundaries are approximated with straight segments along which triangular and pulse functions are defined.

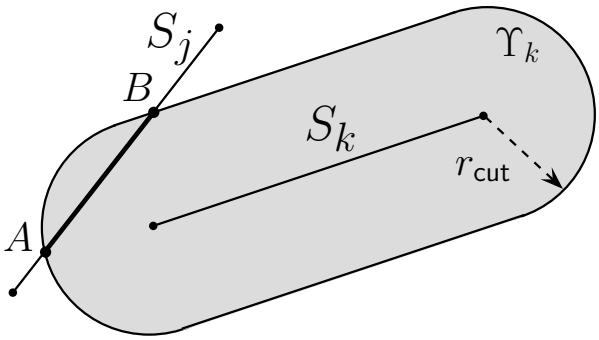

Figure 3. Test integration interval AB, where the interactions from segment S_k are non-negligible.

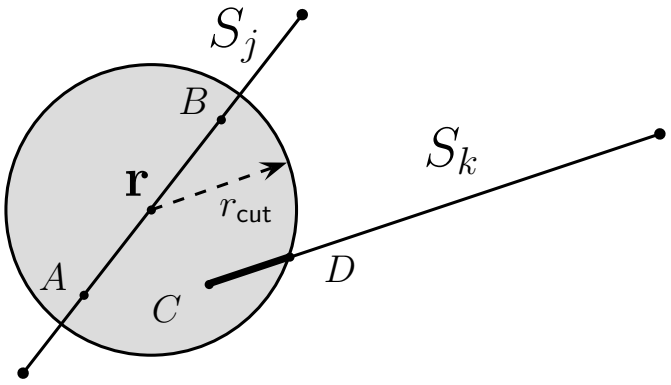

Figure 4. Basis integration interval CD, for test point $\mathbf{r}$.

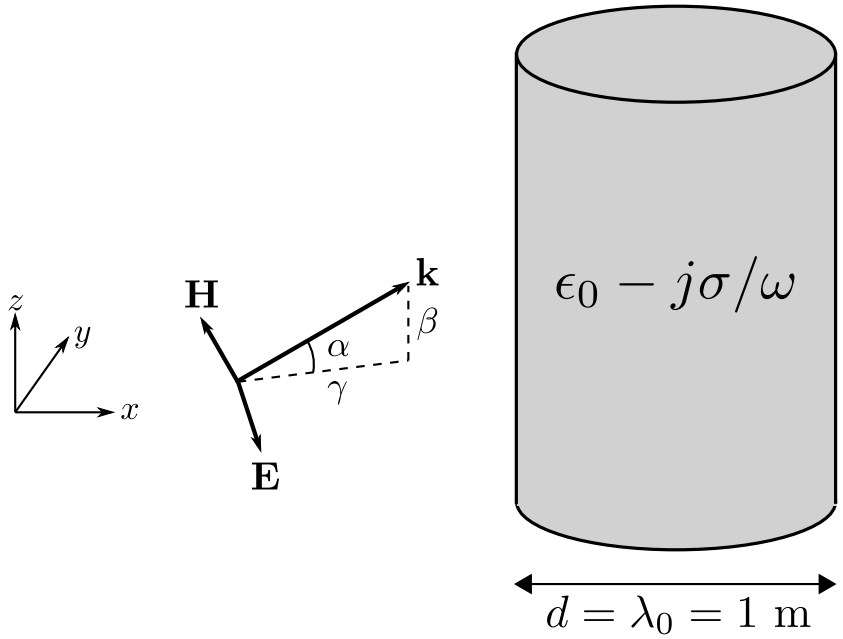

Figure 5. Plane wave scattering at a conductive cylinder with conductivity σ, permittivity $\epsilon_0 - j\sigma/\omega$ and diameter $d = 1$ m. The cylinder is illuminated by a linearly polarized plane wave, with free space wavelength $\lambda_0 = 1$ m, impinging at an angle α w.r.t. the (x, y) plane.

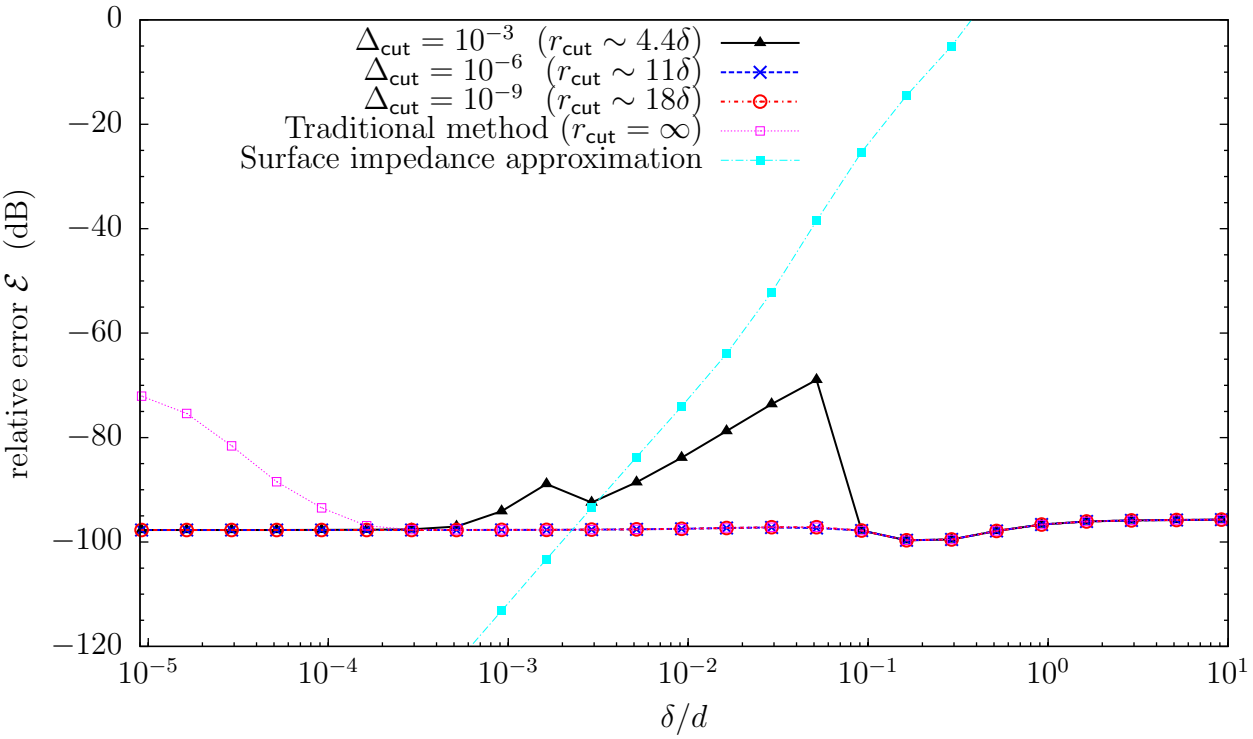

Figure 6. Relative error of the co-polarization RCS (VV) as a function of the skin depth δ for oblique incidence ($\alpha = 45°$) for the proposed method, the traditional method without cutoff distance and limited extracted part, and a surface impedance approximation. The quadrature order of the interaction integrals ($Q = 32$) and number of boundary segments ($N = 630$) are constant.

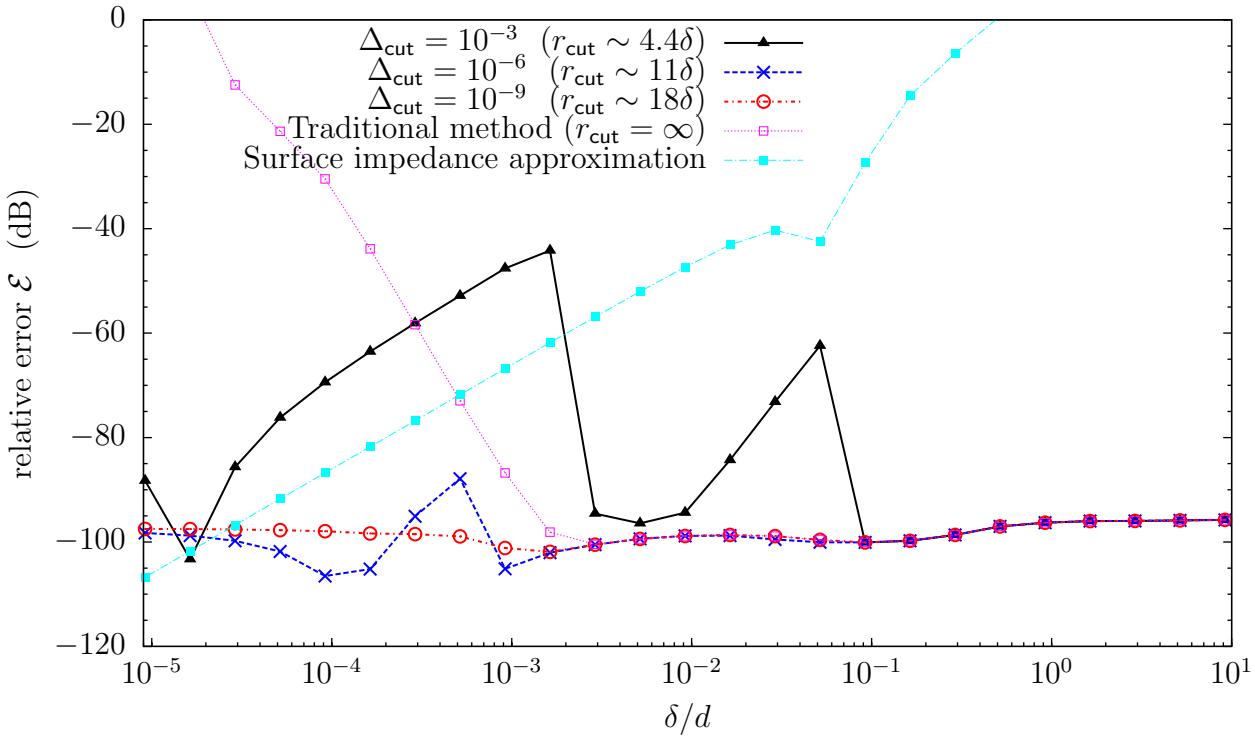

Figure 7. Relative error of the cross-polarization RCS (VH) as a function of the skin depth δ for oblique incidence ($\alpha = 45°$) for the proposed method, the traditional method without cutoff distance and limited extracted part, and a surface impedance approximation. The quadrature order of the interaction integrals ($Q = 32$) and number of boundary segments ($N = 630$) are constant.

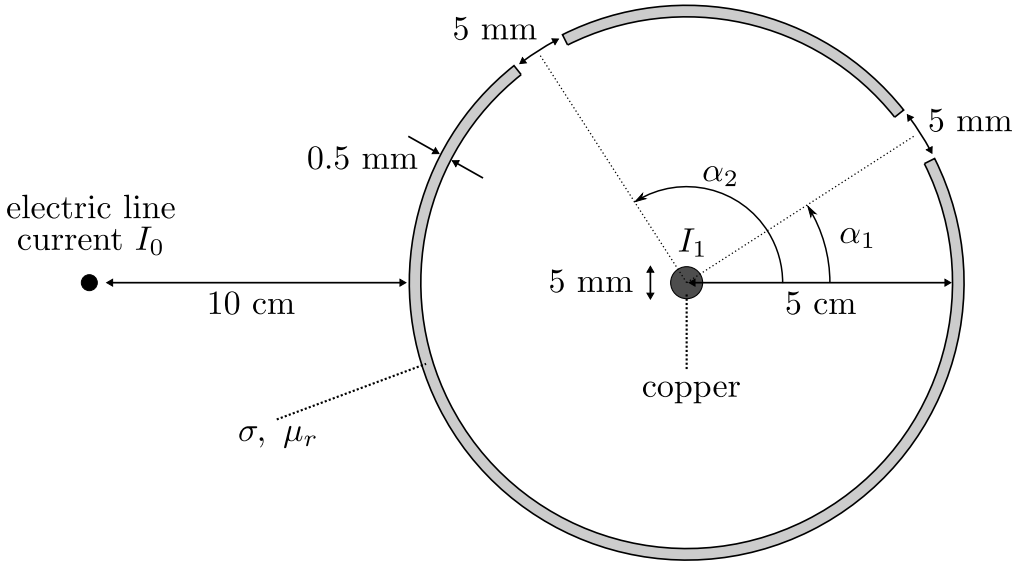

Figure 8. Cross section of a coaxial enclosure with conductivity σ and relative permeability μ_r, illuminated by an electric line current I_0, and enclosing a copper signal conductor with induced noise current I_1. There are one or two slots present at angles α_1 and α_2.

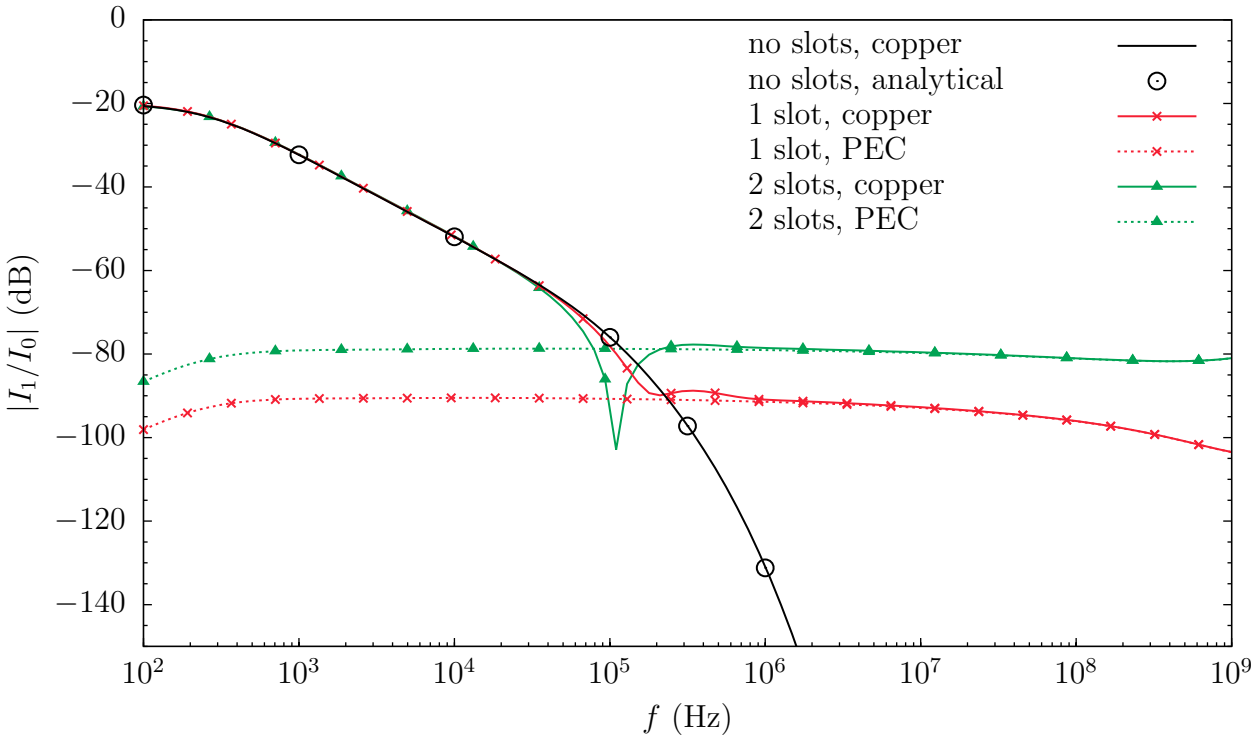

Figure 9. Shielding performance of the coaxial enclosure as a function of frequency, for a copper and perfect electric conducting (PEC) enclosure, with a varying number of slots.

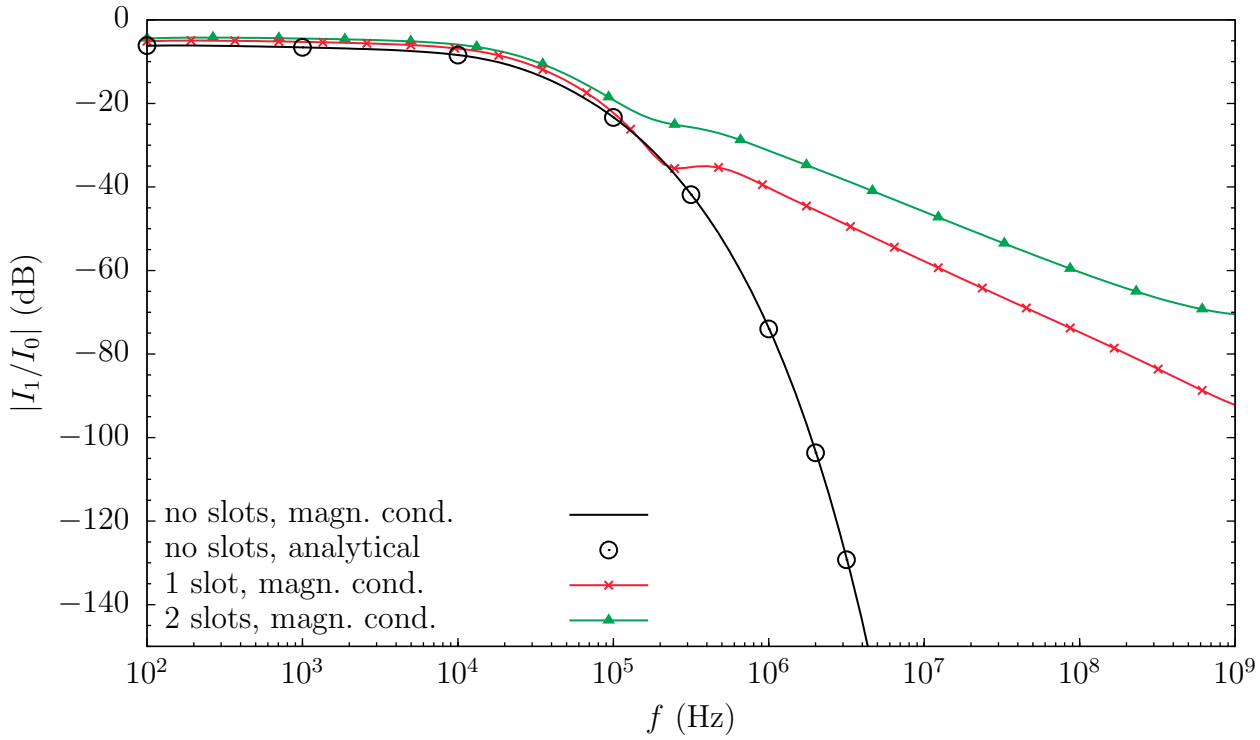

Figure 10. Shielding performance of the coaxial enclosure as a function of frequency, for the magnetic conductor, with a varying number of slots.

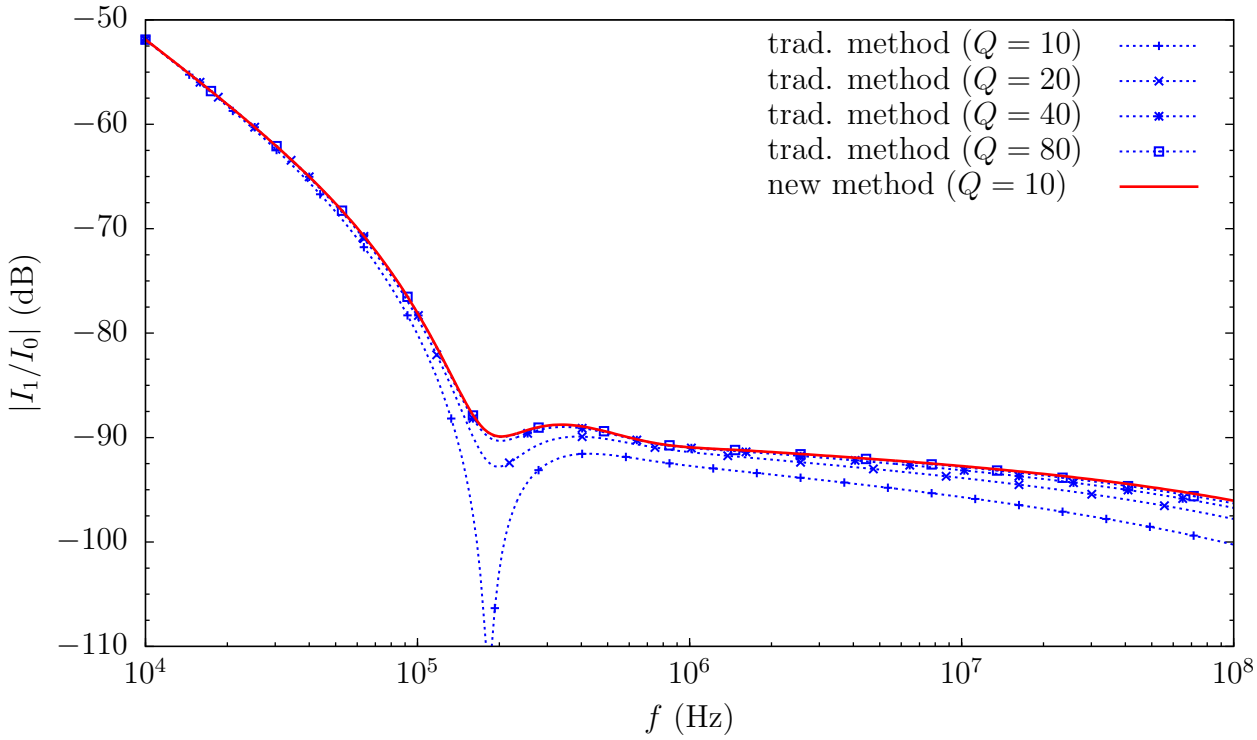

Figure 11. Comparison between the traditional method (with $r_{\mathsf{cut}} = \infty$) and the new method in this work (with $\Delta_{\mathsf{cut}} = 10^{-9}$), of the calculated shielding performance of the copper coaxial enclosure with two slots, for a varying quadrature order Q.

Table 1. Simulation time of the new method (top) and the traditional method (bottom), versus the quadrature order Q (see Fig. 11).

Q	Time (s)
10	10
10	17
20	45
40	150
80	575

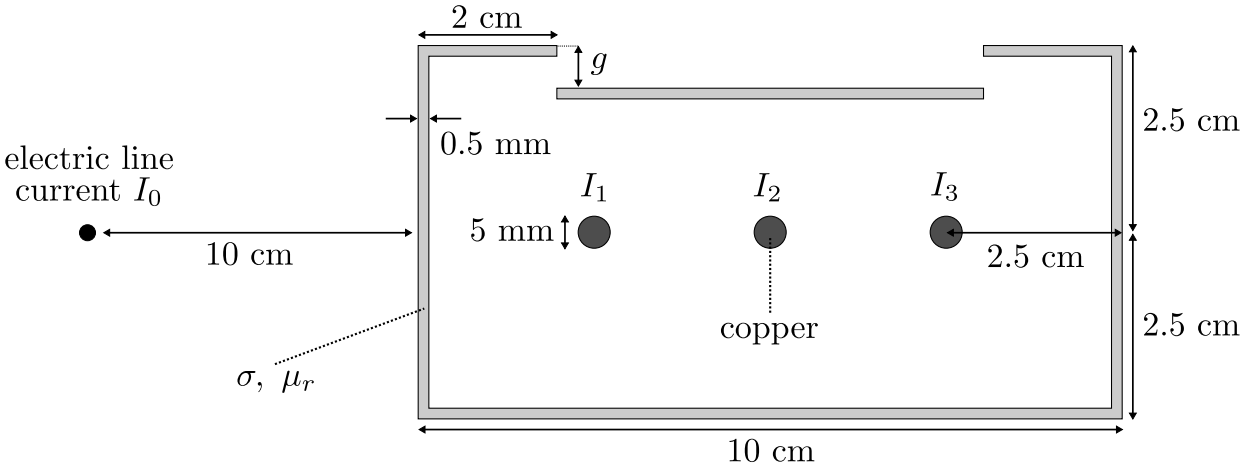

Figure 12. Cross section of an open cable tray with conductivity σ and relative permeability μ_r, illuminated by an electric line current I_0, and enclosing three copper signal conductors with induced noise currents I_1 to I_3. The geometry is symmetrical w.r.t. a vertical line through the center of the middle conductor.

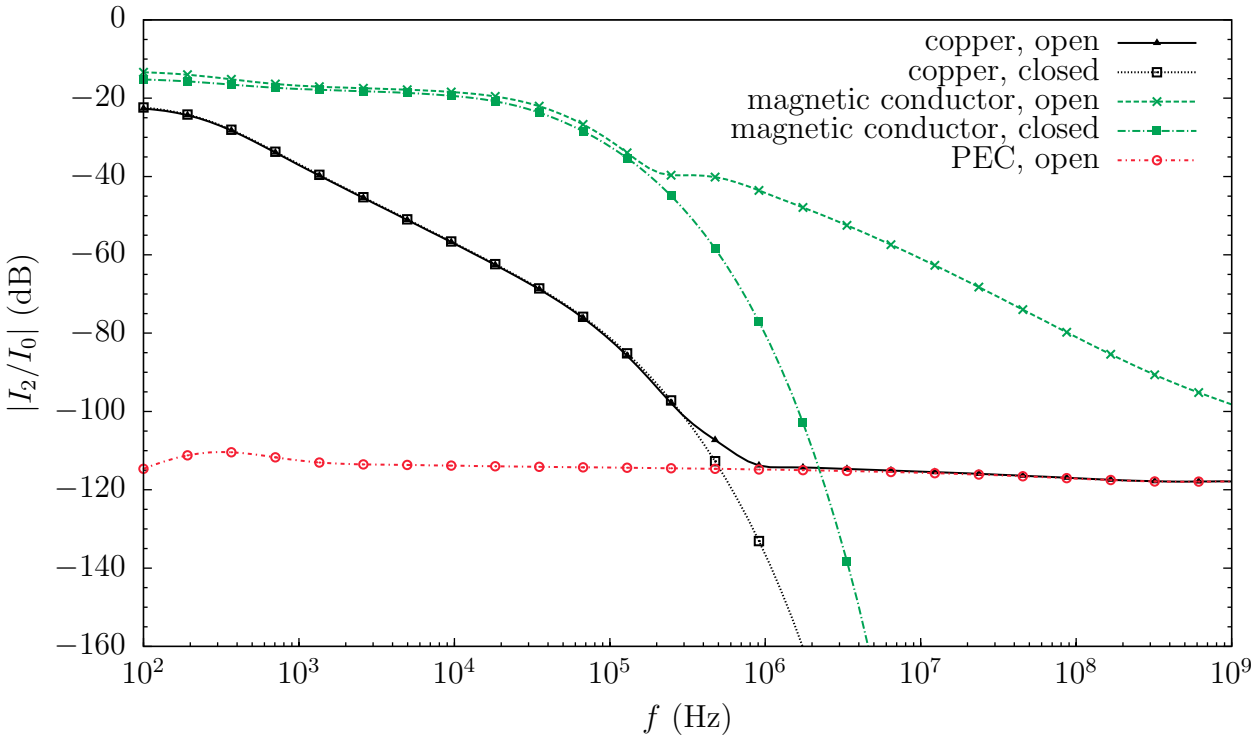

Figure 13. Shielding performance of the open ($g = 5.5$ mm) and closed ($g = 0$) cable tray as a function of frequency, for various shielding materials.

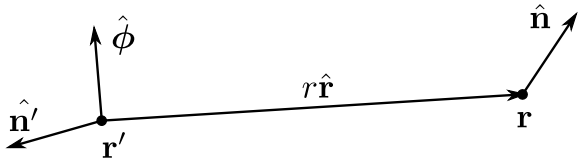

Figure 14. Relevant to the derivation of the normal derivatives.